



# Dynamic regulation of Pep-induced immunity through post-translational control of defence transcript splicing

Keini Dressano, Philipp R. Weckwerth<sup>®</sup>, Elly Poretsky<sup>®</sup>, Yohei Takahashi, Carleen Villarreal, Zhouxin Shen<sup>®</sup>, Julian I. Schroeder<sup>®</sup>, Steven P. Briggs and Alisa Huffaker<sup>®</sup> <sup>™</sup>

The survival of all living organisms requires the ability to detect attacks and swiftly counter them with protective immune responses. Despite considerable mechanistic advances, the interconnectivity of signalling modules often remains unclear. A newly characterized protein, IMMUNOREGULATORY RNA-BINDING PROTEIN (IRR), negatively regulates immune responses in both maize and *Arabidopsis*, with disrupted function resulting in enhanced disease resistance. IRR associates with and promotes canonical splicing of transcripts encoding defence signalling proteins, including the key negative regulator of pattern-recognition receptor signalling complexes, CALCIUM-DEPENDENT PROTEIN KINASE 28 (CPK28). On immune activation by Plant Elicitor Peptides (Peps), IRR is dephosphorylated, disrupting interaction with *CPK28* transcripts and resulting in the accumulation of an alternative splice variant encoding a truncated CPK28 protein with impaired kinase activity and diminished function as a negative regulator. We demonstrate a new mechanism linking Pep-induced post-translational modification of IRR with post-transcriptionally mediated attenuation of CPK28 function to dynamically amplify Pep signalling and immune output.

nnate immunity has been described as a double-edged sword, providing essential protection in the face of attack, but detrimental to the host if allowed to persist<sup>1</sup>. Accordingly, immune responses are tightly regulated by complex layers of dynamic checks and balances. Rapid and reversible modulation of the signalling components requisite for this dynamic regulation commonly occurs through post-transcriptional, translational and post-translational mechanisms without requiring de novo transcription<sup>2-9</sup>. Collectively, these mechanisms rapidly modulate signalling pathways through stochiometric changes in the relative quantities or functional states of key regulators. However, the elucidation of how these regulatory layers assemble into defined modules, particularly with respect to temporal dynamics and cause–effect relationships, remains challenging.

Pattern-recognition receptors (PRRs) recognize microbe-, herbivore- and parasitic-plant-associated molecular patterns, as well as endogenous elicitors, to activate regulatory signalling networks that promote innate immune responses as a first line of defence 10,11. After the initiation of pattern-triggered immunity, endogenous plant hormones and messenger signals amplify the initial inputs to coordinate immune outputs<sup>11</sup>. Among these outputs, Plant Elicitor Peptides (Peps) have emerged as fundamental regulators of innate immunity across higher plants, with a demonstrated ability to enhance resistance to a broad spectrum of insects, pathogens and nematodes in diverse species  $^{12-18}$ . Peps are proteolytically released from PROPEP precursor proteins by the cysteine protease METACASPASE4, and activate PEP RECEPTORs (PEPRs) to coordinate downstream signals that trigger plant immune responses mediating resistance<sup>12,19-24</sup>. Signalling by PEPRs requires SOMATIC EMBRYOGENESIS RECEPTOR KINASE coreceptors and the plasma-membrane-associated kinase BOTRYTIS-INDUCED KINASE 1 (BIK1)<sup>25-29</sup>. Acting as a positive regulator of downstream responses mediated by both reactive oxygen species (ROS) and WRKY transcription factors, BIK1 is rate

limiting for signalling through PRR complexes (including PEPRs) and is continuously turned over to maintain signalling homeostasis<sup>30–32</sup>. The E3 ligases PLANT U-BOX PROTEINS PUB25 and PUB26 facilitate turnover by ubiquitylating BIK1 (ref. <sup>33</sup>). The phosphorylation of conserved residues in BIK1 and in PUB25/PUB26 by CALCIUM-DEPENDENT PROTEIN KINASE 28 (CPK28) enhances ubiquitin ligase activity and promotes BIK1 degradation. Through this mechanism, CPK28 negatively regulates immune receptor signalling by promoting BIK1 turnover<sup>32,33</sup>.

Here we define a new dynamic regulatory mechanism acting on the CPK28 buffering system mediated by an RNA-binding protein, termed IMMUNOREGULATORY RNA-BINDING PROTEIN (IRR). In the absence of immune challenge, IRR associates with CPK28 transcripts to promote canonical splicing into messenger RNA encoding full-length, functional proteins. On the activation of PEPRs, IRR is transiently dephosphorylated, causing dissociation from CPK28 transcripts. The disruption of IRR interaction with CPK28 transcripts leads to increased levels of a retained-intron (RI) variant encoding a truncated protein that lacks EF-hand domains required for the calcium-induced stimulation of kinase activity and exhibiting reduced functionality. Altered ratios of canonical versus RI CPK28 transcripts modulate PEPR signalling sensitivity, with proportional increases in the RI variant, resulting in amplified immune signalling and defence. These dynamic events directly link PEPR-induced dephosphorylation of IRR with post-transcriptionally mediated attenuation of CPK28 function, providing a rapid mechanism to modulate PEPR signalling capacity and immune outputs.

#### Results

**Pep signalling promotes IRR dephosphorylation.** To uncover post-translationally modified regulators of immunity, we examined

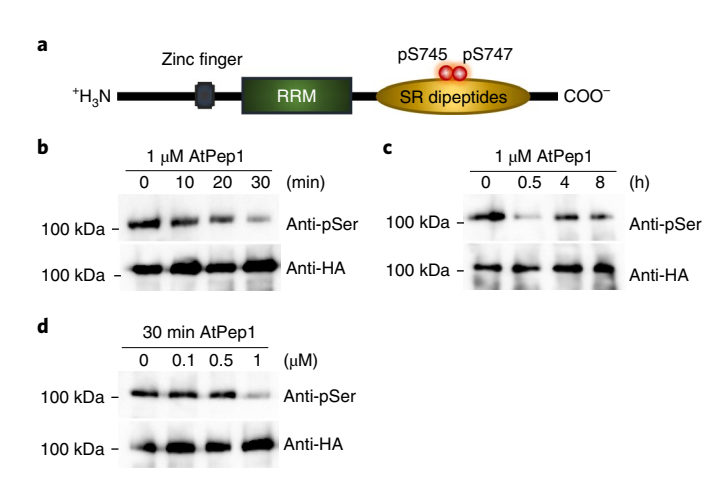


**Fig. 1** | AtPep1 affects the phosphorylation of IRR in a time- and concentration-dependent manner. **a**, IRR phosphorylation sites affected by AtPep1 treatment. **b**, **c**, p35S-IRR-3xHA plants were treated with 1 μM solutions of AtPep1 for 0, 10, 20 and 30 min (**b**) or 0, 0.5, 4 and 8 h (**c**). **d**, p35S-IRR-3xHA plants were treated with 0, 0.1, 0.5 and 1 μM solutions of AtPep1 for 30 min. IRR protein was subjected to immunoblot analysis with anti-phosphoserine (anti-pSer) and anti-HA antibodies. The experiments in **b-d** were repeated three times independently, with similar results.

rapid Pep-induced protein phosphorylation changes in both *Arabidopsis* and maize. Suspension-cultured cells from each species were treated for 10 min with 100 nM *Arabidopsis thaliana* Pep1 (AtPep1) or *Zea mays* Pep3 (ZmPep3), respectively, and analysed in comparison with water-treated controls using nano-liquid chromatography with tandem mass spectrometry<sup>34</sup>. In both species, a predicted RNA-binding protein containing an RNA recognition motif (RRM), IRR, was significantly dephosphorylated (P < 0.02 and P < 0.04, respectively) after Pep treatment (Supplementary Fig. 1), indicating a possible regulatory role in Pep-induced signal transduction across species. Encoded by the At3g23900 and GRMZM2G132936 genes in *Arabidopsis* and maize, respectively, IRR contains zinc finger and RRM domains with a carboxyl-terminal region highly enriched in serine/arginine (SR) dipeptides (Fig. 1a).

To confirm the Pep-induced dephosphorylation of IRR in planta, Arabidopsis lines expressing a triple-tagged fusion of IRR with the human influenza hemagluttinin peptide epitope (HA) were treated with AtPep1, followed by IRR immunoprecipitation and anti-phosphoserine antibody immunoblot analyses of phosphorylation state. Decreased IRR phosphorylation was observed within 30 min of AtPep1 treatment (Fig. 1b), while control anti-HA western blots demonstrated no change in total IRR protein levels. AtPep1-induced dephosphorylation was transient, with a recovery to resting levels of IRR phosphorylation within 4h (Fig. 1c). Decreased IRR phosphorylation also occurred in a concentration-dependent manner (Fig. 1d). To confirm that phosphorylation detected by western blot corresponded to the serine residues observed in the initial phosphoproteomic study, S745 and S747, phospho-abolishing alanine substitutions at these positions were generated. Compared with the wild-type (Wt) IRR fusion protein, the phospho-abolishing variant (IRRS745A,S747A-YFP) showed constitutively decreased phosphorylation (Supplementary Fig. 2). To determine whether AtPep1-induced dephosphorylation was specific to IRR, the phosphorylation of an unrelated SR-rich RRM protein previously reported as a phosphoprotein<sup>35</sup>, SR45, was examined after Pep treatment using plants expressing an SR45-3xHA fusion protein (Supplementary Figs. 3 and 4). SR45 negatively regulates glucose and abscisic acid signalling during early seedling development, and recent transcriptional profiling studies have implicated

it as a negative regulator of innate immunity<sup>36,37</sup>. The phosphorylation levels of SR45 protein were unaltered by AtPep1 treatment (Supplementary Fig. 4), demonstrating that AtPep1-mediated dephosphorylation is not a general phenomenon in SR-rich RRM proteins.

Loss-of-function irr mutants display enhanced Pep-induced **immune responses.** To examine the effects of IRR loss of function on AtPep1 response output, two transfer DNA (T-DNA) insertional knockout mutants of IRR (SALK\_015201, termed irr-1, and SALK\_066572, termed irr-2) were analysed for altered sensitivity to AtPep1 treatment in comparison with an SR45 insertional mutant line (SALK\_123442) as a control. The presence of T-DNA insertions and absence of target gene expression were confirmed for all lines by PCR (Supplementary Fig. 5). Under normal growth conditions in soil or on tissue culture medium, both irr knockout lines were developmentally and morphologically indistinguishable from Wt. However, both irr knockout lines demonstrated visible growth differences in the presence of AtPep1, which inhibits primary root elongation in Arabidopsis seedlings<sup>22,24</sup>. Wt Col-0 seedlings grown in media supplemented with 0.1 µM AtPep1 have primary roots approximately half the length of those of seedlings grown on water-supplemented medium (Fig. 2a), while the PEPR double-knockout line, pepr1 pepr2, which is fully insensitive to AtPeps, demonstrates no root growth inhibition after AtPep1 treatment. In contrast, the primary roots of irr1-1 and irr1-2 were significantly shorter than Wt roots when grown on medium supplemented with both 0.1 µM and 1 μM AtPep1, indicating hypersensitivity to the peptide (Fig. 2a and Supplementary Fig. 6a), whereas sr45 primary root growth was indistinguishable from Wt (Supplementary Fig. 6b). This result indicated a potential role for IRR as a negative regulator of AtPep1-induced responses. Additional layers of signalling and output downstream of AtPep1 were investigated, including the production of secondary messengers, kinase activation and the relative expression of AtPep1-associated marker genes. AtPep1 promotes the generation of secondary-messenger ROS through the stimulation of NADPH oxidase activity within minutes of PEPR activation<sup>22,38</sup>. While the timing of AtPep1-induced ROS production was the same in both Wt and irr knockouts, the magnitude of ROS generated was greater in irr lines (Fig. 2b and Supplementary Fig. 7a). AtPep1 treatment also stimulates the phosphorylation-mediated activation of MAP KINASES (MPK) 3, 6 and 4/11, which are integral to many plant signalling pathways responsive to biotic and abiotic stresses<sup>39,40</sup>. MPK3/6/4/11 activation after AtPep1 treatment was probed through western blotting with anti-phospho-p44/42 MAP kinase antibody, revealing that the phosphorylation of MPK3, MPK6 and MPK4/11 was more intense and prolonged in *irr* knockouts than in Wt, with detectable activity continuing 60 min after Pep treatment (Supplementary Fig. 7b). In correspondence with the upregulation of second messenger and MAP kinase activities, the expression of the AtPep1-responsive marker genes PLANT DEFENSIN 1.2 (PDF1.2) and PATHOGENESIS-RELATED PROTEIN 1 (PR-1) was also significantly increased 24h after AtPep1 treatment in irr knockouts compared with Wt (Fig. 2c,d)12. The expression of the AtPep1-induced marker gene TYROSINE AMINOTRANSFERASE 3 was also observed as marginally increased in irr mutants, but was not statistically significant (Supplementary Fig. 7c). The irr-1 knockout phenotype was rescued through complementation with the IRR gene driven by its native promoter: two independent lines expressing pIRR-IRR-YFP in the irr-1 background behaved as Wt plants in assays of AtPep1-induced root growth inhibition and ROS production (Supplementary Fig. 8).

To assess whether enhanced AtPep1-induced immune responses in *irr* lines translated to increased disease resistance, plants were challenged with both the hemibiotrophic bacterial pathogen *Pseudomonas syringae* pv. *tomato* DC3000 (*Pst* DC3000) and

the necrotrophic fungal pathogen Botrytis cinerea. When inoculated with Pst DC3000 by leaf infiltration, bacterial proliferation was similar in both Wt and irr-1 plants after two and five days (Supplementary Fig. 9a), whereas the pepr1 pepr2 double mutant was more susceptible to Pst DC3000, as previously reported24. In contrast, after inducing immunity through the pre-infiltration of leaves with AtPep1 24h before Pst DC3000 inoculation, bacterial proliferation was significantly reduced in irr-1 and irr-2 knockout plants when compared with Wt (Fig. 2e). On being challenged with B. cinerea, four days post-inoculation, the average lesion area of irr leaves was smaller than for Wt (Supplementary Fig. 9b). Correspondingly, the quantification of fungal proliferation through quantitative PCR with reverse transcription (qRT-PCR) analysis of the relative ratios of B. cinerea Cutinase A DNA versus A. thaliana GAPDH DNA revealed significantly lower pathogen levels in both irr mutant lines compared with Wt (Fig. 2f). To examine whether irr lines were hypersensitive to another peptide elicitor of immune responses, flg22-induced responses were evaluated (Supplementary Fig. 10). Interestingly, the irr lines did not display increased flg22 sensitivity as measured by root growth inhibition and ROS accumulation. Furthermore, compared with Wt, the irr lines did not have enhanced flg22-induced resistance to Pst DC3000 two days post-inoculation, and showed only marginal decreases in proliferation after five days. Together this indicates that IRR-based negative regulation more strongly affects AtPep1 signalling than flg22 and that IRR may have varying degrees of influence depending on immune input.

To investigate IRR function in maize, a virus-induced gene silencing (VIGS) system derived from Foxtail mosaic virus (FoMV) was deployed to silence ZmIRR (Supplementary Fig. 11a,b)41. Maize var. B73 seedlings were biolistically inoculated with FoMV-derived vectors carrying two different IRR sequence fragments, designated as FoMV-IRR-1 and FoMV-IRR-2. Control plants were inoculated with FoMV vector carrying no insert (FoMV-V). For each FoMV construct, ten plants confirmed as infected were selected for further analysis. To evaluate relative ZmIRR silencing, ZmIRR transcript levels were compared among leaves of plants infected with FoMV-IRR-1/2, empty vector FoMV-V and uninoculated control plants using qRT-PCR. The expression levels of ZmIRR were similar in uninoculated and FoMV-V-infected maize plants, demonstrating that FoMV-V infection alone did not significantly affect ZmIRR gene expression (Fig. 2g). However, infection with either of the FoMV-IRR constructs significantly reduced ZmIRR expression (Fig. 2g). As irr knockout Arabidopsis mutants are hypersensitive to AtPep1, maize FoMV ZmIRR knockdown plants were tested

for sensitivity to ZmPep3. In maize, ZmPep3 is a potent inducer of herbivore-associated volatile organic compounds (VOCs) that serve as indirect defences by recruiting parasitic wasps to attack lepidopteran herbivore pests feeding on leaves<sup>14</sup>. VOC emissions from FoMV-infected maize leaves after ZmPep3 treatment were measured by gas chromatography, and total VOCs emitted after peptide treatment were significantly higher from maize plants inoculated with FoMV-IRR-1/2 than from control plants (Fig. 2h). A direct comparison of relative *ZmIRR* expression with total VOC emission levels in FoMV-IRR-1/2 confirmed that lower *ZmIRR* expression correlated with higher VOC emission (Supplementary Fig. 11c,d). Together these experiments suggest that IRR functions as a negative regulator of Pep-induced immune responses in both *Arabidopsis* and maize.

*irr* knockouts exhibit broad changes in defence gene expression and splicing patterns. To better understand potential mechanisms underlying *irr* hypersensitivity to Pep treatment, global transcriptional patterns in *irr-1* and Wt plants were profiled by RNA-seq 24h post-treatment with either water or 1 μM AtPep1. Water-treated *irr-1* plants demonstrated extensive dysregulation of genes relating to the immune response, with over 600 genes differentially regulated in *irr-1* compared with Wt (Supplementary Fig. 12 and Supplementary Table 1). Analysis of Gene Ontology (GO) for transcripts with increased basal expression levels in *irr-1* revealed substantial enrichment of immunity-related terms, with the top categories including response to stimulus, defence response, immune system process and programmed cell death (Fig. 3a and Supplementary Table 2).

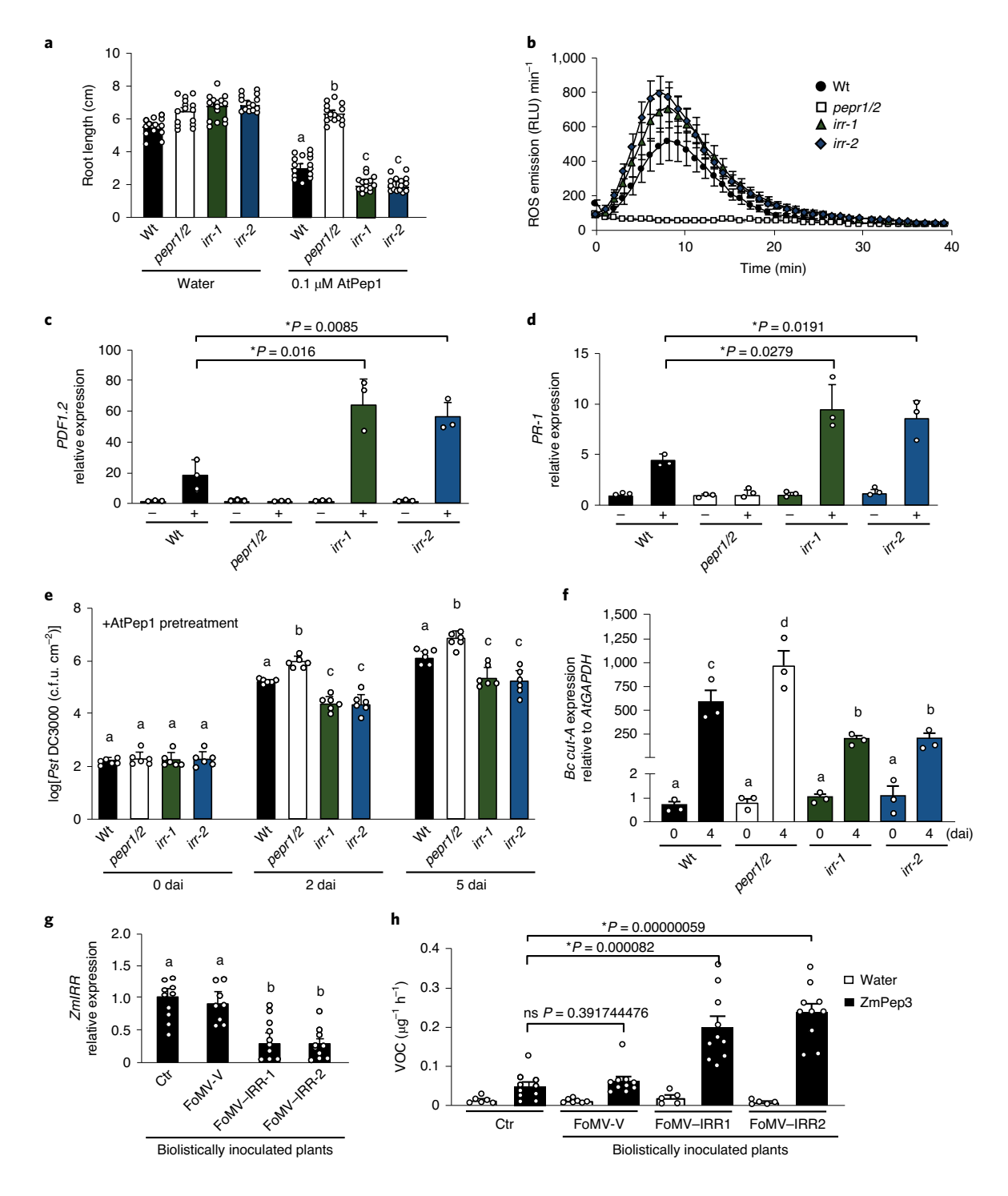
RNA-binding proteins with SR enrichment and RRM domains are established as key to precursor mRNA (pre-mRNA) processing and alternative splicing in eukaryotes<sup>42,43</sup>; thus, we considered related roles for IRR. Notably, widespread changes in splicing patterns were observed in irr-1 compared with Wt, with differences in RI, alternative 3' splice site, skipped-exon, alternative 5' splice site and mutually exclusive exon events (Fig. 3b and Supplementary Table 3). Among the alternative splicing patterns observed in the irr-1 knockout, RI events were the most abundant. Numerous transcripts encoding defence-signalling proteins exhibited differing ratios of RI variants encoding premature stop codons that would predictably result in truncated proteins and potentially modified functions (Supplementary Fig. 13). Negative regulators of plant immune signalling, such as CPK28, LESION-SIMULATING DISEASE 1 (LSD1) and JASMONATE-ZIM-DOMAIN PROTEIN 4 (JAZ4) all exhibited increased levels of RI transcripts, whereas a

Fig. 2 | IRR mutants are hypersensitive to AtPep1 treatment. a, Arabidopsis seedlings were treated with water or a solution of 0.1μM AtPep1, and root length measured after 15 days of treatment. The values represent the mean ± s.d. of 15 seedlings. b, Total ROS production was registered continuously using luminol fluorescence for 40 min after the addition of 0 or 1 µM AtPep1, then summed. The values are the mean ± s.e.m. of the relative light units (RLU) emitted. c,d, The relative expression levels of the AtPep1-inducible genes PDF1.2 (c) and PR-1 (d) were determined by real-time qRT-PCR using mRNA from entire seedlings treated with water (-) and a solution of 1µM AtPep1 (+) for 24 h. The values represent the fold change in expression versus the water-treated Wt samples after normalization against GAPDH expression. The error bars indicate the s.d. of three biological replicates. e, Pst DC3000 infection assay of Wt, pepr1 pepr2 (pepr1/2), irr-1 and irr-2 plants after pretreatment via infiltration with a solution of 1µM AtPep1 24 h before infection. The bars indicate colony-forming units (c.f.u.) for samples immediately after inoculation (0) or two and five days after inoculation (dai). The error bars indicate s.d.; n=6. f, B. cinerea infection in Wt, pepr1 pepr2 and irr mutants. The quantification of in planta growth of B. cinerea is shown. qPCR was used to analyse the relative levels of B. cinerea Cutinase A genomic DNA (Bc cut-A) compared with Arabidopsis GAPDH (AtGAPDH). The error bars indicate s.d.; n=15. The experiments in **a-f** were repeated at least three times independently, with similar results. **g**, Analysis of ZmIRR gene expression in maize plants carrying FoMV-based VIGS constructs targeting ZmIRR (FoMV-IRR-1 and FoMV-IRR-2) relative to empty viral vectors (FoMV-V) and uninoculated control plants (Ctr). The bar graphs display the relative expression levels of ZmlRR mRNA in leaf 5 as determined by real-time qRT-PCR. The values represent the fold change in expression versus the uninoculated Ctr samples after normalization against ZmRPL17 expression. h, Total VOCs from maize leaves inoculated with VIGS constructs targeting ZmIRR (FoMV-IRR-1 and FoMV-IRR-2) relative to empty viral vectors (FoMV-V) and uninoculated control plants (Ctr). VOCs were measured 16 h post-treatment with water or with a 5 µM solution of ZmPep3. All error bars indicate the s.d. of five to ten biological samples. The experiments in g and h were repeated two times independently, with similar results. For all graphs, the different letters represent significant differences (one-way analysis of variance (ANOVA) followed by Tukey's test corrections for multiple comparisons; P < 0.05). The asterisks indicate significant differences using Student t-tests (two-tailed distribution, unpaired), with P < 0.05; ns, not significant.

NATURE PLANTS | VOL 6 | AUGUST 2020 | 1008-1019 | www.nature.com/natureplants

positive regulator of immunity, CYSTEINE-RICH RECEPTOR-LIKE KINASE 13 (*CRK13*) had markedly decreased levels of an RI isoform<sup>32,44-47</sup> (Supplementary Fig. 14a). To validate the occurrence of RI events observed through RNA-seq analysis, qRT-PCR was performed with primer sets unique to the introns of target genes that were retained at different ratios in *irr-1* and Wt plants. Amplification of the RI variant was performed in parallel with amplification using primers for the canonical splice form so that the relative ratios could be compared. These analyses confirmed that in the *irr-1* mutant, the ratios of *CPK28*, *LSD1* and *JAZ4* RI splice variants increased compared with Wt, whereas the ratio of *CRK13* RI splice variant decreased (Supplementary Fig. 14b).

In support of a role in mRNA splicing, IRR has been predicted to physically interact with the CC1-LIKE SPLICING FACTOR encoded by At2g16940 (ref. <sup>48</sup>). Using a yeast two-hybrid system with the coexpression of IRR and CC1 fused to bipartite transcription factor halves, IRR was found to physically interact with CC1 as predicted (Fig. 3c). The coexpression of CC1 with SR45, which has been demonstrated to mediate pre-mRNA splicing, also yielded a positive interaction<sup>49</sup> (Supplementary Fig. 15). Because the *sr45* knockout does not share the AtPep1-hypersensitive phenotype of *irr* knockouts, we conclude that while CC1 interaction with these proteins probably facilitates function, it is unlikely to contribute to target specificity.



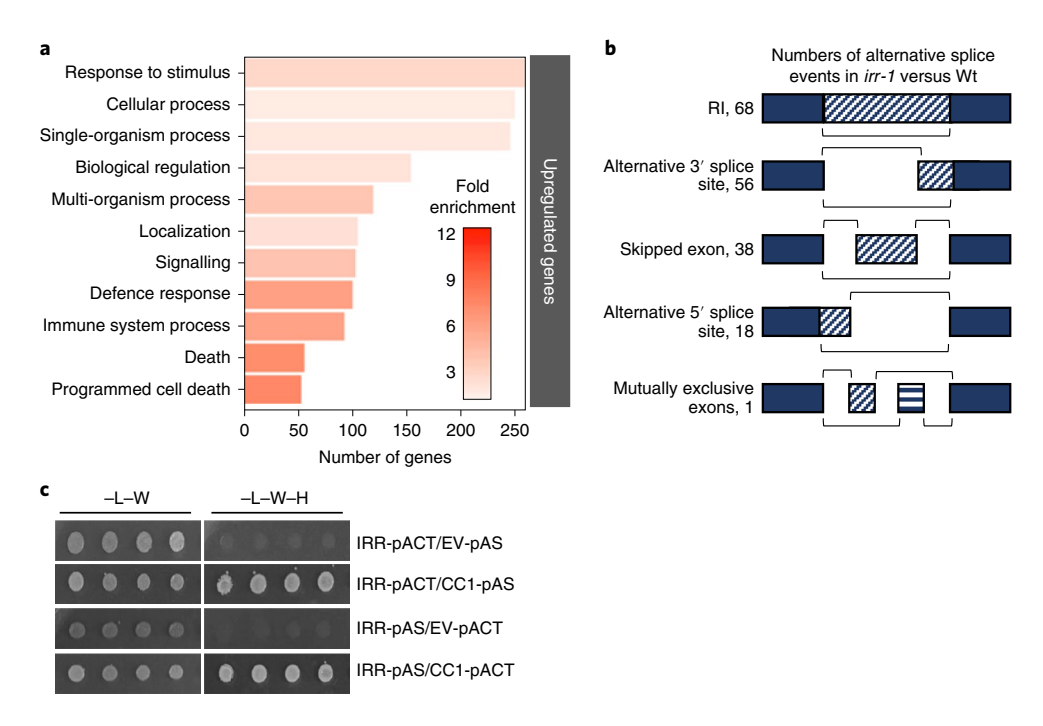


**Fig. 3 | IRR** is **implicated in defence and alternative splicing. a**, GO term distribution of genes for which expression is upregulated in *irr-1* versus Wt plants, as analysed through RNA-seq. **b**, Numbers of alternative splice events in *irr-1* versus Wt. Three biological replicates for each sample group were analysed. **c**, IRR interacts with CC1-splicing factor in yeast. Yeast strain AH109 was cotransformed with IRR and CC1-splicing factor encoding proteins. The transformants were selected in media lacking leucine and tryptophan (–L–W), and interaction was tested in media lacking leucine, tryptophan and histidine (–L–W–H). This experiment was performed three times, with similar results.

The CPK28-RI splice variant underlies reduced negative regulation. RI variants of transcripts encoding CPK28 were among the most significantly increased alternative splicing events observed in irr-1 knockouts, with a relative abundance of CPK28-RI approximately fivefold higher than in Wt plants, while the levels of canonically spliced CPK28 remained unchanged (Fig. 4a). Given the known function of CPK28 in negatively regulating AtPep1-PEPR complex activity by promoting the turnover of the rate-limiting component BIK1, the role of IRR-mediated changes in CPK28 transcript splicing was examined<sup>32,33</sup>. CPKs are most commonly activated through the exposure of the catalytic site as a result of conformational changes triggered by calcium ion binding to the four regulatory EF hand domains<sup>50,51</sup>. Partial losses of these EF hand domains can inhibit Ca2+-induced conformational changes, resulting in inactive CPKs with shielded catalytic domains<sup>50</sup>. The truncated CPK28 protein encoded by the CPK28-RI splice variant lacks two C-terminal EF hands (Fig. 4b) and was predicted to exhibit compromised catalytic activity compared with full-length CPK28. The production of truncated CPK28 from CPK28-RI was confirmed through the expression of complementary DNA encoding either canonical CPK28 or CPK28-RI as both a YFP fusion in Arabidopsis and a GST fusion in Escherichia coli. In both cases, western blotting revealed that CPK28-RI was expressed to yield a truncated fusion protein of the expected size (Fig. 4c,d). Using in vitro kinase activity assays, GST-CPK28 actively auto-phosphorylated and trans-phosphorylated both GST- and histidine-tagged BIK1 protein, as well as the catalytically inactive variant GST- and His-BIK1<sup>K105A/K106A</sup> (refs. <sup>27,32</sup>), whereas GST-CPK28-RI had greatly reduced phosphorylation activity (Fig. 4d and Supplementary Fig 16a). To deduce whether CPK28-RI was potentially active if exposed to higher levels of Ca2+, kinase activity was observed with a titration of Ca<sup>2+</sup> concentrations up to 100 µM. Even as Wt CPK28 showed increasing kinase activity as Ca2+ levels were increased, CPK28-RI activity remained attenuated (Supplementary Fig 16b).

To ascertain whether CPK28-RI had reduced regulatory function in vivo, the *cpk28* knockout mutant was complemented with either *CPK28* or *CPK28*-RI expressed under control of the native promoter (Supplementary Fig. 16c). As determined by total ROS production, the AtPep1-hypersensitive phenotype of *cpk28* was rescued through complementation with pCPK28-CPK28-YFP, but the expression of pCPK28-CPK28-RI-YFP did not reduce sensitivity to AtPep1 (Supplementary Fig. 16d)<sup>32</sup>.

We hypothesized that one potential mechanism underlying irr-1 hypersensitivity to AtPep1 treatment is reduced negative regulation of PEPR signalling by CPK28 due to a loss of IRR function in promoting canonical splicing of CPK28 transcript to produce a functional full-length protein. In this case, increased expression of the canonical CPK28 transcript should fully or partially rescue the *irr-1* phenotype. To test this hypothesis, Arabidopsis plants were transformed with cDNA constructs encoding both CPK28 transcript variants in the irr-1 mutant background under the control of the native promoter and fused to a YFP tag. Two independent events for each transformation were selected, and protein expression was confirmed by western blot, with plants expressing pCPK28-CPK28-RI-YFP producing a smaller protein than plants expressing pCPK28-CPK28-YFP (Fig. 4c). The expression of CPK28 transcript was approximately doubled in irr-1/pCPK28-CPK28-YFP plants compared with Wt and irr-1, and the expression of CPK28-RI transcript in irr-1/pCPK28-CPK28-RI-YFP plants was comparable to that in *irr-1* (Supplementary Fig. 17)

AtPep1-induced resistance to *Pst* DC3000 was examined in *irr-1* plants expressing pCPK28-CPK28-YFP versus pCPK28-CPK28-RI-YFP. Without AtPep1 pretreatment, bacterial proliferation in *irr-1* expressing YFP-tagged CPK28 or CPK28-RI was similar to that in Wt (Supplementary Fig. 18). As previously observed, when pretreated with AtPep1 24h before inoculation, *irr-1* knockout plants were more resistant to *Pst* infection than Wt as measured by decreased bacterial proliferation after two days. In AtPep1-pretreated

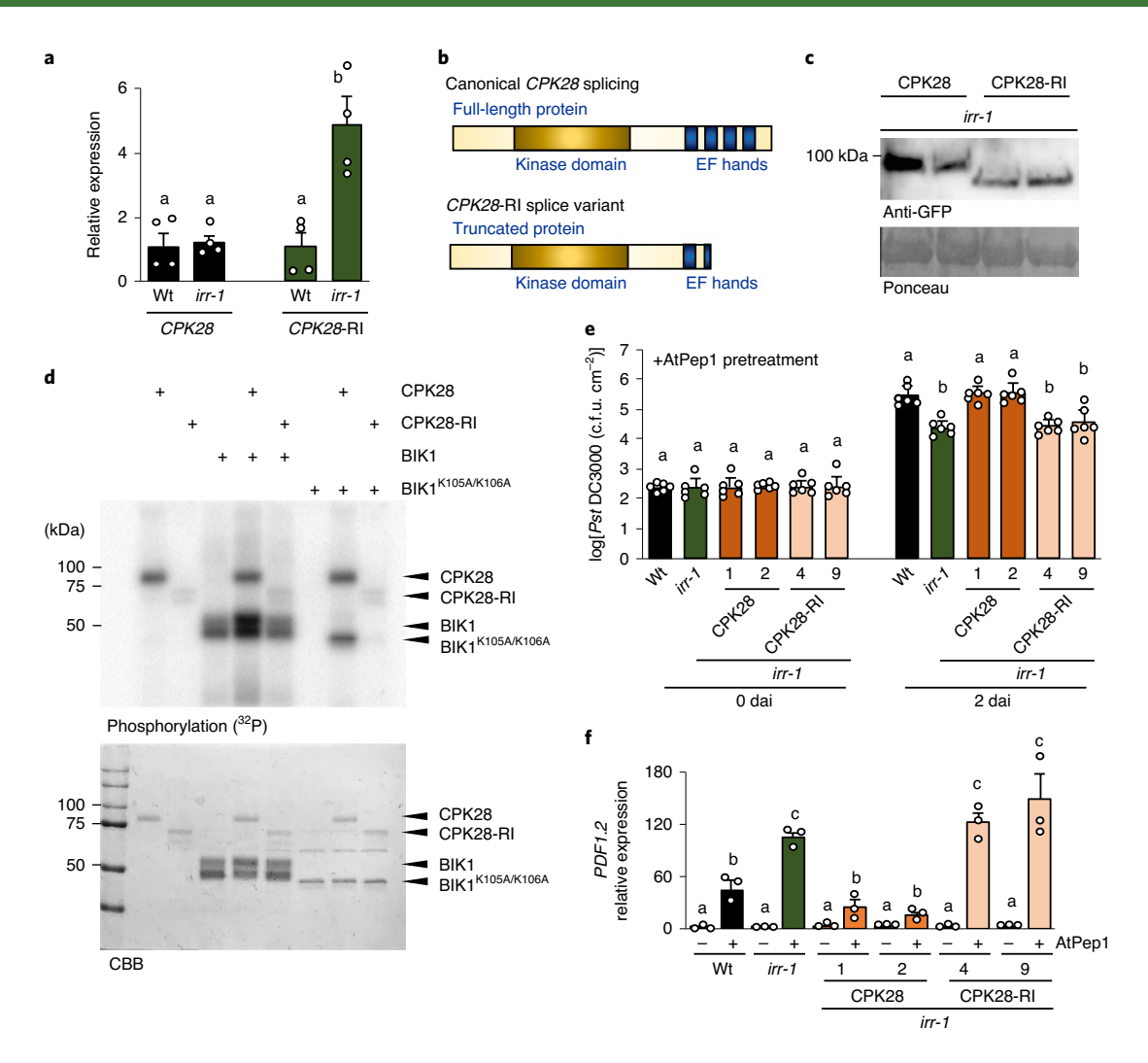


**Fig. 4 | IRR** affects the ratio of *CPK28*-RI splice variants and *CPK28* function. **a**, Relative expression of *CPK28* and *CPK28*-RI splice variant in *irr-1* plants. The values represent the fold change in expression versus the Wt control samples after normalization against *ACTIN2* expression. The error bars indicate s.e.m.; n = 4. **b**, Schema representing proteins translated from canonically spliced *CPK28* transcript, which encodes a full-length protein containing four EF hands, versus the *CPK28*-RI splice variant, encoding a truncated protein missing two EF hands. **c**, Detection of CPK28-YFP and CPK28-RI-YFP fusion proteins as separated on a 7.5% SDS-PAGE gel using western blotting. Proteins were extracted from leaves of transgenic plants expressing pCPK28-CPK28-YFP and pCPK28-RI-YFP in the *irr-1* background. Anti-GFP antibody was used to detect both proteins. Two independent events per line were analysed. CPK28-YFP, 85 kDa; CPK28-RI-YFP, 75 kDa. Ponceau staining was used for the verification of protein loading. **d**, Autoradiograph showing the incorporation of <sup>32</sup>P into GST-fused CPK28 and His-fused BIK1 recombinant proteins after in vitro kinase assays. Coomassie Brilliant Blue (CBB) stains are included as controls. **e**, *Pst* DC3000 infection assay of Wt, *irr-1*, *irr-1*/pCPK28-CPK28-YFP and *irr-1*/pCPK28-CPK28-RI-YFP plants performed 24 h post-infiltration with a 1 μM solution of AtPep1. The bars indicate samples 0 and 2 dai. The error bars indicate s.d.; n = 6. **f**, Relative expression levels of *PDF1.2* as determined by real-time qRT-PCR for mRNA from entire seedlings treated for 24 h with water (—) or a solution of 1 μM AtPep1 (+). The values represent the fold change in expression versus the water-treated Wt control samples after normalization against *ACTIN2* expression. The error bars indicate the s.d. of three biological replicates. The different letters represent significant differences (one-way ANOVA followed by Tukey's test corrections for multiple comparisons; P < 0.05). The e

irr-1 plants expressing pCPK28-CPK28-YFP, Pst proliferation was similar to that in Wt, confirming that increased levels of canonical CPK28 transcript were able to rescue the irr-1 phenotype (Fig. 4e). In contrast, the expression of pCPK28-CPK28-RI-YFP in irr-1 did not reduce the AtPep1-hypersensitive phenotype, as these lines exhibited the same enhanced AtPep1-induced restriction of bacterial proliferation as irr-1. AtPep1 sensitivity of irr-1 lines expressing pCPK28-CPK28-YFP was further examined through the analysis of AtPep1-induced PDF1.2 marker gene expression. In irr-1 plants expressing pCPK28-CPK28-YFP, PDF1.2 expression was similar to that in Wt, whereas irr-1 lines expressing pCPK28-CPK28-RI-YFP maintained elevated PDF1.2 expression

similar to *irr-1* (Fig. 4f). These experiments confirmed that increased levels of canonical *CPK28* transcript was able to reduce the AtPep1-hypersensitive phenotype of *irr-1*. Taken together, the evidence indicates that truncated CPK28-RI protein is not fully functional as a negative regulator, and the inability of *irr* knockout plants to promote canonical *CPK28* splicing for the production of a functional full-length protein that negatively regulates PEPR signalling may be a substantial contributor of *irr* hypersensitivity to AtPep1. Furthermore, the relief of CPK28-mediated negative regulation of immunoregulatory receptor complex signalling seems integral to plant defence responses: inoculation with *Pst* also triggers an increased proportion of *CPK28*-RI transcripts (Supplementary Fig. 19),

demonstrating that *CPK28* alternative splicing occurs during the course of a natural plant–microbe interaction.

Accumulation of CPK28-RI transcript is dependent on the phosphorylation state of IRR. To ascertain whether levels of the CPK28-RI splice variant were affected by Pep signalling, plants were treated with AtPep1, and the relative abundances of CPK28 and CPK28-RI transcripts were analysed by qRT-PCR. Notably, AtPep1 promoted significant increases in proportional CPK28-RI levels at 30 min (Fig. 5a), temporally coinciding with peak AtPep1-induced dephosphorylation of IRR (Fig. 1c). Elevated proportions of CPK28-RI returned to the initial levels after 4h (Fig. 5a), concurrent with the recovery of IRR phosphorylation post-AtPep1 treatment. To determine whether the IRR phosphorylation state contributed to CPK28-RI accumulation, irr-1 plants overexpressing an HA-tagged fusion of the phospho-abolishing mutant of IRR, IRR<sup>S745A,S747A</sup>, were examined. The *irr-1*::IRR<sup>S745A,S747A</sup>–3xHA plants exhibited higher levels of CPK28-RI than Wt or irr-1::IRR-3xHA plants, demonstrating a phenotype equivalent to irr-1 knockout plants (Fig. 5b). The inability of IRR<sup>S745A,S747A</sup> to reduce proportional CPK28-RI levels in the irr-1 background supports the dephosphorylation of IRR as a contributing factor to the accumulation of CPK28-RI variant transcripts after AtPep1 treatment. Similarly, IRR<sup>S745A,S747A</sup> failed to rescue the AtPep1-hypersensitive phenotype of irr-1. The expression of the AtPep1-induced marker gene PDF1.2 remained elevated in irr-1::IRRS745A,S747A-3xHA lines, whereas irr-1 lines complemented with IRR phenocopied Wt (Fig. 5c). Furthermore, irr-1::IRR<sup>S745A,S747A</sup>–3xHA plants exhibited enhanced AtPep1-induced restriction of Pst proliferation comparable to irr-1, whereas Pst proliferation in irr-1::IRR-3xHA plants was similar to that in Wt (Fig. 5d). Like in irr-1 lines, the basal resistance to Pst of both irr-1::IRRS745A,S747A-3xHA and irr-1::IRR-3xHA was unchanged from Wt (Supplementary Fig. 20). Together these results suggest that phosphorylated IRR acts as a negative regulator of AtPep1-induced immune responses. In unchallenged Wt plants, the population of IRR protein is predominantly phosphorylated on pS745 and pS747, and active as a negative regulator. However, on perception of AtPep1, the transient dephosphorylation of IRR temporarily attenuates negative regulatory function. When IRR is absent, as in irr knockouts, IRR-mediated negative regulation is fully relieved and results in enhanced immune responses.

IRR associates with CPK28 transcript in a phosphorylationdependent manner. To better understand how the dephosphorylation of IRR might contribute to its function, the behaviour of the IRR<sup>\$745A,\$747A</sup> mutant protein relative to Wt IRR was assessed. The subcellular localization of YFP-tagged IRR<sup>S745A,S747A</sup> was examined and compared with that of IRR-YFP, and found to be unaffected (Supplementary Fig. 21). For many SR-rich RNA-binding proteins that function in pre-mRNA processing, phosphorylation promotes interaction with other proteins in the splicing complex<sup>52</sup>, so the effect of mutant IRR<sup>S745A,S747A</sup> on physical interactions with the CC1 splicing factor was also examined. As determined by plate-based yeast two-hybrid and the monitoring of yeast growth dynamics in a liquid medium, the mutation of the phosphorylation sites to alanine does not impair interactions with the CC1-splicing factor, nor does it alter interaction affinity (Supplementary Fig. 22a-c). To investigate whether AtPep1-induced dephosphorylation affects IRR stability and turnover, irr-1 plants overexpressing triple HA-tagged IRR were treated with AtPep1. No change in total IRR protein levels was observed by western blot after AtPep1 treatment (Supplementary Fig. 23a). However, cotreatment with AtPep1 and the proteasome inhibitor MG132, or the protein translation inhibitor cycloheximide (CHX), revealed that the phosphorylation state may affect the turnover rate. Treatment with MG132 or CHX alone did not affect IRR levels, but with cotreatments, IRR accumulated

30 and 120 min after MG132/AtPep1 treatment, and was depleted after CHX/AtPep1 treatment (Supplementary Fig. 23a,b). Mutant IRR<sup>S745A,S747A</sup> protein levels were significantly decreased by CHX treatment in both the absence and presence of AtPep1, suggesting that the dephosphorylation of IRR promotes protein turnover (Supplementary Fig. 23c).

To ascertain whether IRR regulation of CPK28 transcript splicing might occur through the association of the two in complex, RNA immunoprecipitation (RIP) coupled with PCR analysis was used to test for IRR-CPK28 transcript interactions. RIP-PCR demonstrated that IRR associates with CPK28 mRNA, with a CPK28 fragment amplified from RNA coimmunoprecipitating with IRR (Fig. 5e). Whether this association is direct or occurs through complex with additional factors is not known. The RNA-binding protein SR45 was used as a negative control, since SR45-interacting transcripts have previously been identified by RIP-seq, and CPK28 is not among them<sup>53</sup>. As expected, the amplification of RNA coimmunoprecipitated with SR45 did not yield a CPK28 fragment, nor did the amplification of RNA coimmunoprecipitated with an unfused triple-HA tag (Fig. 5e). Because mutant IRR<sup>\$745A,\$747A</sup> fails to promote canonical splicing of CPK28, in contrast to Wt IRR, the dependence of the IRR-CPK28 interaction on pS745 and pS747 was probed. No CPK28 fragment was amplified from RNA coimmunoprecipitation with IRRS745A,S747A (Fig. 5e), indicating that abolished phosphorylation at these sites disrupts the association of IRR with CPK28 transcript in addition to eliminating IRR-stimulated canonical splicing of CPK28. All proteins were detected after protein-RNA complex immunoprecipitation (Supplementary Fig. 24).

Because phospho-abolishing mutations of IRR also abolished the association of IRR with CPK28 transcript, the effects of AtPep1-mediated transient dephosphorylation of IRR on CPK28 transcript interactions were investigated. Coimmunoprecipitation of triple HA-tagged IRR with associated RNA was performed 0, 0.5 or 4h post-treatment with AtPep1 to compare with IRR dephosphorylation dynamics (Fig. 1a,b). CPK28 transcript was abundant in IRR-interacting RNA at 0h, but declined in RNA coimmunoprecipitated with IRR 30 min after AtPep1 treatment (Fig. 5f). The AtPep1-induced dephosphorylation of IRR thus parallels a disrupted association with CPK28 transcript. Predictably, 4h after AtPep1 treatment, when IRR phosphorylation levels have recovered (Fig. 1b), increased amplification of CPK28 transcript from coimmunoprecipitated RNA was observed, indicating a re-establishment of IRR-CPK28 association (Fig. 5f). For all samples, input and coimmunoprecipitated RNA was determined to be of similar quantities, and CPK28 transcript amplified similarly from input RNA collected from samples before coimmunoprecipitation (Fig. 5e,f).

## Discussion

Alternative splicing is a fundamental layer of regulation in eukaryotes, allowing for rapid adaptation to stress in the absence of de novo transcription. For both plants and animals, immune challenge is associated with widespread changes in splicing patterns, with pathogen infection, caterpillar infestation and elicitor treatments all resulting in the large-scale reprogramming of plant mRNA splicing<sup>54-58</sup>. SR-rich RRM-containing (SR-RRM) proteins in particular have been implicated as potential regulators of immune-induced variation in splicing<sup>37,57,59,60</sup>. The disruption of function or of proper trafficking of SR-RRM proteins can result in the dysregulation of both stress-induced splicing patterns and disease resistance<sup>37,59,60</sup>. The critical role of SR-RRM proteins in regulating plant immunity is underscored by the finding that pathogens such as *Phytophthora* sojae have evolved effector proteins that physically interact with SR-RRM proteins to alter immune-induced splicing patterns and promote susceptibility<sup>61</sup>. Transcripts for many defence signalling proteins have been identified as targets of alternative splicing during immunity, including PRRs, kinases, transcription factors and

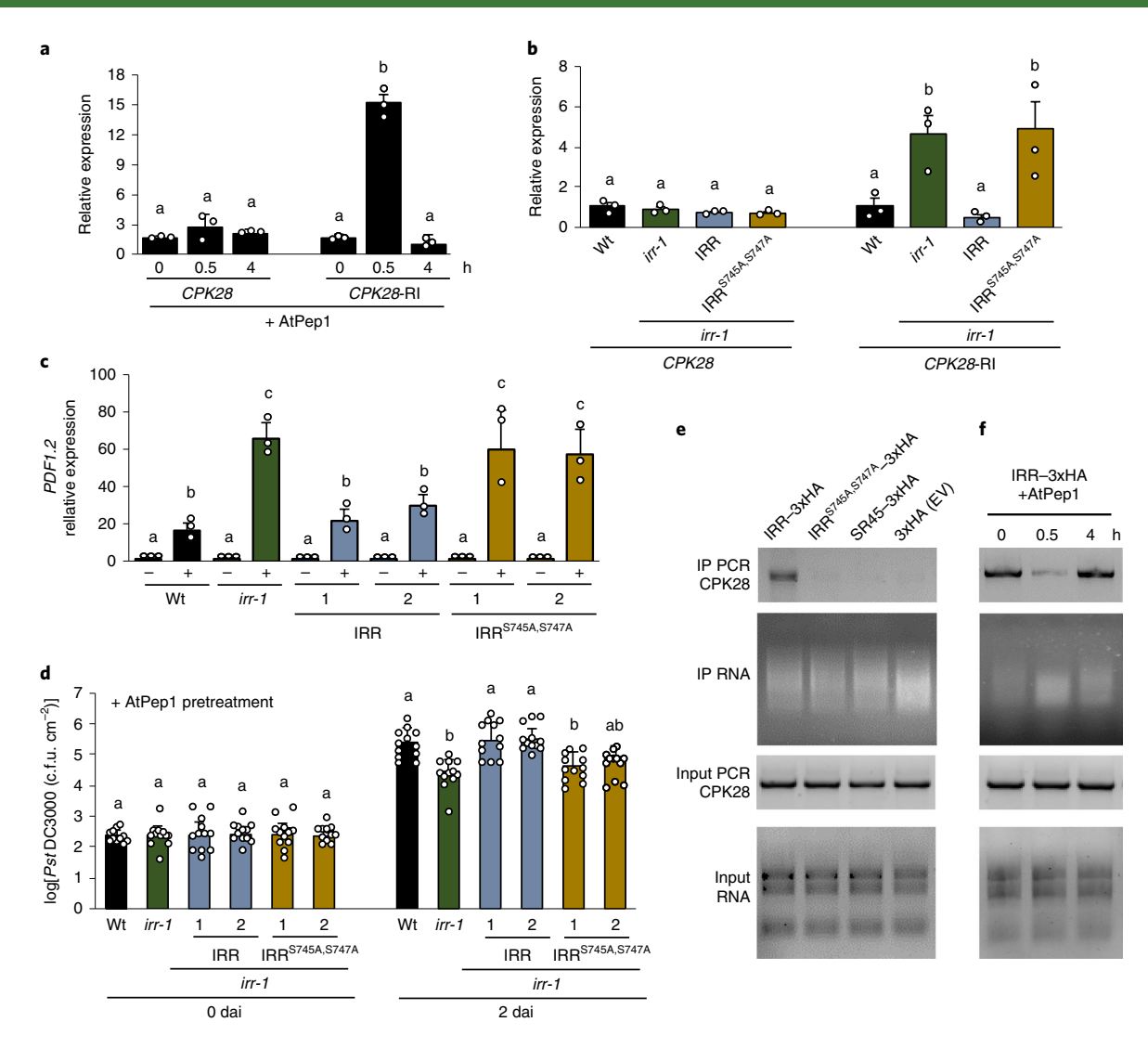
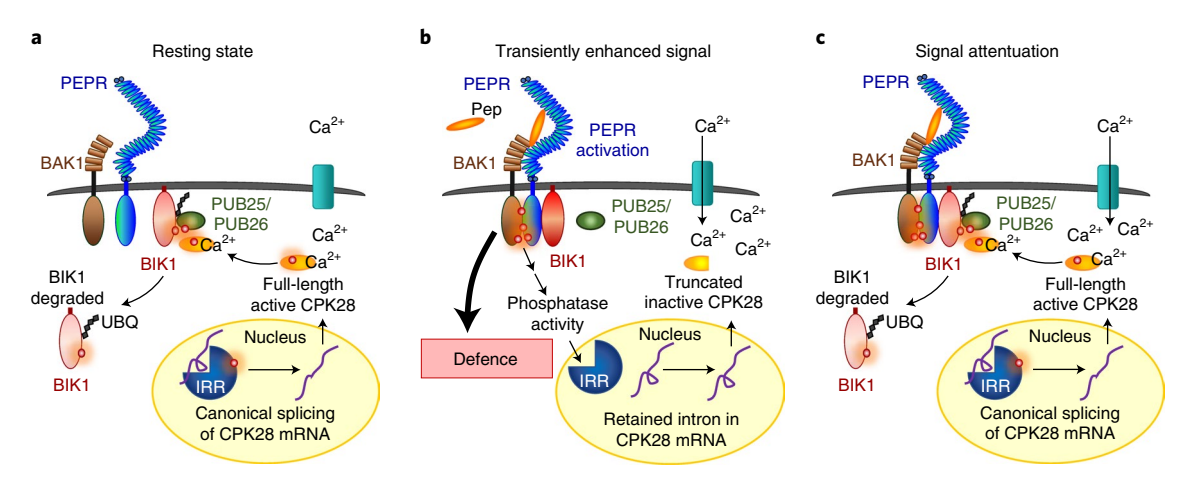


Fig. 5 | Association of IRR with CPK28 transcript is phosphorylation-dependent. a, Relative expression of CPK28 and CPK28-RI splice variant in irr-1::IRR-3xHA lines analysed by qRT-PCR. The plants were treated with solutions of 1µM AtPep1 for 0, 0.5 or 4h. The values represent the fold change in expression versus 0 h samples after normalization against ACTIN2 expression. The error bars indicate s.e.m.; n = 3. b, Relative expression of CPK28 and CPK28-RI in Wt, irr-1 and transgenic lines overexpressing triple HA-tagged IRR (irr-1::IRR) and IRR<sup>S745A,S747A</sup> (irr-1::IRR<sup>S745A,S747A</sup>). The values represent the fold change in expression versus the Wt control samples after normalization against ACTIN2 expression. c, The relative expression of AtPep1-inducible gene PDF1.2 was determined by real-time qRT-PCR using mRNA from whole seedlings treated for 24 h with either water (–) or a 1μM solution of AtPep1 (+). The values represent the fold change in expression versus the water-treated Wt control samples after normalization against ACTIN2 expression. Two independent events per transgenic line overexpressing triple HA-tagged IRR (irr-1::IRR) and IRR<sup>\$745A,\$747A</sup> (irr-1::IRR\$745A,\$747A}) were used. The error bars indicate the s.d. of three biological replicates. d, Pst DC3000 infection assay of Wt, irr-1 and irr-1 overexpressing triple HA-tagged IRR (irr-1::IRR) and IRR<sup>S745A,S747A</sup> (irr-1::IRR<sup>S745A,S747A</sup>) plants 24 h after pretreatment by infiltration with a 1 µM solution of AtPep1. The bars indicate samples 0 and 2 dai. The error bars indicate s.d.; n=11-12. e, RIP from transgenic plants overexpressing IRR-3xHA, IRR<sup>5745A,5747A</sup>-3xHA, SR45-3xHA and 3xHA (empty vector, EV). RIP-PCR was performed to detect CPK28 transcripts. f, RIP from transgenic plants overexpressing IRR-3xHA after treatment with a 1μM solution of AtPep1 for 0, 0.5 or 4 h. RIP-PCR was performed to detect CPK28 transcripts. The protein-RNA complex was immunoprecipitated using anti-HA magnetic beads. Input RNA was extracted from all samples as a control. PCR reactions with primers to detect CPK28 transcript used cDNA templates reverse transcribed from input RNA samples. The different letters represent significant differences (one-way ANOVA followed by Tukey's test corrections for multiple comparisons; P < 0.05). The experiments were repeated three times independently, with similar results.

Resistance proteins<sup>2,58,60,62-64</sup>. RI events are frequently observed, with the retention of early introns often associated with changes in transcript stability or translation, and the retention of later introns generally resulting in the production of truncated protein isoforms<sup>2,55,62</sup>. For truncated signalling protein variants that have been characterized, function is generally abolished or altered, supporting a role for alternative splicing as one mechanism to quickly remodel signalling pathways and the resultant cellular output<sup>2,55</sup>. Interestingly, altered levels of several *CPK28* splice variants

(including those with RIs) have recently been reported after flg22 treatment in an MPK4-dependent manner<sup>58</sup>. While this indicates that *CPK28* splicing is a common regulatory target for multiple inputs, our finding that flg22-induced responses are only modestly affected in *irr* knockouts, along with similar findings for *cpk28* knockouts, indicates that flg22-induced *CPK28* splicing may regulate sensitivity to signals other than flg22 (ref. <sup>32</sup>). The examination of the degree of intersection between these and other MAMP/DAMP signalling pathways will be an interesting line of research for the future.



**Fig. 6 | Proposed model by which IRR dynamically regulates CPK28 immunomodulatory buffering of PEPR-mediated immunity. a**, Resting state: phosphorylated IRR associates with transcripts encoding CPK28, facilitating canonical splicing into mRNA that produces a full-length protein. This protein functions as a negative regulator of immune receptor complex signalling by phosphorylating PUB25/26 ubiquitin ligases to promote the ubiquitylation and subsequent degradation of BIK1. **b**, Transiently enhanced signal: AtPep1 activates PEPR receptor complexes, leading to the transient dephosphorylation of IRR and dissociation from *CPK28* transcripts. This results in the temporary accumulation of an RI variant encoding a premature stop codon that yields a truncated and inactive CPK28 protein variant, reducing CPK28 buffering of the receptor complex and resulting in amplified PEPR-mediated immune signalling and defence output. **c**, Signal attenuation: the recovery of IRR phosphorylation re-establishes the association with CPK28 transcript to promote the canonical splicing and resumed translation of a full-length protein, which reinstitutes the negative regulation of PEPR signalling and immunity.

Previous studies have established alternative splicing as a contributor to immune regulation and have revealed RNA-binding proteins and target transcripts involved in this process. In this study, we have characterized IRR as an RNA-binding protein that regulates defence response strength and have identified IRR-mediated changes in splicing, including targets encoding defence signalling proteins. We have also demonstrated how dynamic and site-specific post-translational modification of IRR regulates the association with and alternative splicing of one of these transcripts, encoding the key defence regulator CPK28, to affect immune response outputs. It is likely that many of the other alternative splicing events observed in irr knockouts also impact immune regulation and contribute to the overall AtPep1-hypersensitive phenotype of irr. For instance, the hyperactivation of MAP kinase phosphorylation observed in irr knockouts has been found to occur through PBS1-like kinases other than BIK1, indicating that some IRR-mediated signalling is dependent on additional factors beyond the CPK28-regulated stability of BIK1 (refs. 65,66). Future analysis of cpk28 irr double mutants will clarify which irr phenotypes are dependent on CPK28. This relationship and additional IRR targets are of interest for future study to increase the overall understanding of both IRR and Pepregulated immunity.

On the basis of our current findings, we propose one model for IRR function, in which IRR dynamically regulates the CPK28 immunomodulatory buffering system (Fig. 6). Before immune challenge, IRR is predominantly phosphorylated at S745 and S747, and associates with CPK28 transcripts, facilitating canonical splicing to produce a full-length, functional protein (Fig. 6a). Full-length CPK28 promotes BIK1 turnover to suppress immune receptor signalling by phosphorylating both BIK1 and the ubiquitin ligases PUB25 and PUB26 to promote BIK1 ubiquitylation and degradation<sup>32,33</sup>. On the Pep-induced activation of PEPRs, IRR is transiently dephosphorylated and dissociates from CPK28 transcripts, resulting in increased levels of the CPK28-RI variant (Fig. 6b). The truncated protein encoded by CPK28-RI lacks EF hand motifs required for the calcium-induced stimulation of kinase activity. Increased levels of this less-active CPK28-RI protein attenuate CPK28-mediated BIK1 degradation and temporarily enhance the signalling capacity of PEPR complexes to amplify defence

outputs. The re-phosphorylation of IRR facilitates equilibration back to immunoregulatory homeostasis, with CPK28 again buffering receptor complex function (Fig. 6c). This study defines a dynamic process that directly links the PEPR-induced dephosphorvlation of IRR with post-transcriptionally mediated attenuation of CPK28 function, revealing a new mechanism to modulate PEPR signalling capacity and immune response outputs. This regulatory module represents a strategy to temporarily derepress immune signalling during the acute response phase for the promotion of a more robust protective response. Although this derepression of signal transmission is transient (on the order of hours), the downstream changes that are activated trigger a more lasting enhanced immunity (on the order of days). In sum, these findings reveal a new layer of complexity in the intricate regulatory programs used by plants to wield the double-edged sword of innate immunity for protection while minimizing the detrimental effects of an inappropriately persistent response.

# Methods

Phosphoproteomic screen. A. thaliana T87 suspension-cultured cells and maize suspension-cultured endosperm cells (var. Black Mexican Sweet) were treated with either water or 100 nM AtPep1 and ZmPep3, respectively. The cells were collected after 10 min into liquid nitrogen. Protein extracted from these samples was subjected to a tryptic digest, labelled with iTRAQ mass tags, mixed and analysed. Phosphopeptides were enriched using CeO<sub>2</sub> affinity capture and analysed separately. Peptides were separated by nano-liquid chromatography using salt gradients on a three-phase capillary column with an LTQ Velos linear ion trap tandem mass spectrometer in positive ion mode and data-dependent acquisitions. The peptides were separated into three mass classes before scanning, and each mass spectrometry scan was followed by five tandem mass spectrometry scans of the most intense parent ions. The data were extracted and searched using Spectrum Mill (Agilent). Peptide abundance and phosphorylation levels were quantified by spectral counting with counts for each protein representing the total number of peptides that match to that protein.

**Phosphorylation assay.** Plants carrying p35S-IRR-3xHA and p35S-SR45-3xHA constructs were grown on plates containing half-strength MS media for 10–15 days, then transferred to half-strength MS liquid media and treated with varying concentrations of AtPep1 (0.1, 0.5 and 1  $\mu$ M) for 30 min, or treated with 1  $\mu$ M AtPep1 for different lengths of time (10 min, 20 min, 30 min, 4h and 8 h). Water treatment was used as a control. After treatment, approximately 1 g of whole seedlings was homogenized in extraction buffer (300 mM sucrose, 100 mM Tris-HCl pH 7.5, 25 mM EDTA, 25 mM NaF, 1 mM Na,MoO<sub>22</sub> 1 mM phenylmethyl

sulfonyl fluoride, 0.5% Triton-X and protease inhibitor cocktail (Sigma), adjusted to pH 5.8–6.2) and centrifuged at 10,000 g for 10 min at 4 °C. The supernatant was transferred to a new microcentrifuge tube, mixed with denaturing 1× loading buffer (NuPAGE LDS buffer) containing 10%  $\beta$ -mercaptoethanol and incubated at 95 °C for 8 min. The proteins were separated by SDS-PAGE and further analysed by western blot. Anti-phosphoserine (1:1,000, Sigma) antibody and anti-mouse-HRP-conjugated secondary antibody (1:2,000, Sigma) were used with the Super Signal West Pico Maximum Chemiluminescent detection kit (Thermo Scientific) to detect proteins. The HA-tagged proteins were detected with anti-HA (1:1,000, Sigma) and anti-mouse HRP (1:1,000, Sigma) antibodies.

Analysis of protein expression and stability. Plants carrying p35S-IRR–3xHA and p35S-IRR<sup>5745A</sup>–3xHA constructs were grown on plates containing half-strength MS media for seven days, then transferred to half-strength MS liquid media and treated with  $1\,\mu\text{M}$  AtPep1 for varying lengths of time as indicated in the figures, or treated with peptide concomitantly with  $10\,\mu\text{M}$  CHX, or with peptide concomitantly with  $50\,\mu\text{M}$  MG132. The solvent dimethylsulfoxide was used as a control. After treatment, 500 mg of plant tissue was homogenized in extraction buffer and centrifuged at  $10,000\,g$  for  $10\,\text{min}$  at  $^{4}$  °C. The supernatant was homogenized with denaturing  $1\times$  loading buffer (NuPAGE SDS buffer) containing 10%  $\beta$ -mercaptoethanol and incubated at  $95\,^{\circ}$  C for 8 min. The proteins were separated by SDS–PAGE and further analysed by western blot. Anti-HA (1:1,000, Sigma) and anti-mouse HRP (1:1,000, Sigma) antibodies were used with the Super Signal West Maximum Chemiluminescent detection kit (Thermo Scientific) to detect proteins.

RNA-seq. Sterile seeds were sown on half-strength MS media for seven to ten days and transferred to 24 well plates containing liquid half-strength MS. Approximately 15 plants were transferred to individual wells. Three hours after transfer, the plants were treated with either water or  $1\,\mu\text{M}$  peptide for 24 h at room temperature and constant light. The plant tissue was collected in liquid nitrogen, and total RNA was isolated with the Spectrum Plant Total RNA kit (Sigma) and treated with the Turbo DNA-free kit (Ambion). RNA quality was checked using the Agilent2100 Bioanalyzer (Agilent Technologies). Three biological replicates per genotype per treatment were used. The preparation of the RNA-seq 250–300-base-pair (bp) insert cDNA library, Illumina HiSeq platform PE150 sequencing and bioinformatic data analysis were performed at the Novogene Corporation. REViGO was used to create the summarized list of significantly enriched GO terms  $^{60}$ .

Yeast two-hybrid. The IRR, SR45 and CC1-splicing factor coding regions were amplified from Arabidopsis cDNA using standard PCR and cloned into the pENTR/D-TOPO vector. To generate the IRR phospho-abolishing mutations, the QuickChange II XL site-directed mutagenesis kit (Agilent Technologies) was used to substitute serine to alanine (S745A, S747A). The fragments were transferred into pACT and pAS vectors by recombination. The primers used to amplify the fragments are listed in Supplementary Table 4. Yeast strain AH109 was transformed with the desired pairs of the pACT and pAS vectors as described in ref. 69. The transformed yeast cells were grown on a synthetic complete medium lacking leucine and tryptophan (Clontech) and selected on a synthetic complete medium lacking leucine, tryptophan and histidine (Clontech). To check the strength of protein-protein interactions, four transformed yeast cells were grown individually in liquid synthetic complete medium lacking leucine, tryptophan and histidine for two days at 29 °C, 200 rpm. Their optical density was measured, adjusted to 0.05, and the cells were transferred to a 96-well plate (250  $\mu$ l per well). The plate was inserted into the microplate reader and agitated once every hour for 30 s. The incubation temperature was 29 °C. The optical density was measured every hour until yeast growth was saturated.

MAP kinase phosphorylation assay. Two-week-old seedlings were treated with  $1\,\mu\text{M}$  solutions of AtPep1 and then collected in liquid nitrogen after 0, 5, 10, 30 and 60 min. The proteins were extracted with Lacus buffer (50 mM Tris–HCl pH 7.5, 10 mM MgCl<sub>2</sub>, 15 mM EGTA, 100 mM NaCl, 1 mM sodium fluoride, 1 mM sodium molybdate, 0.5 mM Na<sub>3</sub>VO<sub>4</sub>, 30 mM  $\beta$ -glycerol-phosphate and 0.1% Triton-X 100), as described previously". The homogenized protein samples were centrifuged at 21,000 g for 20 min at 4 °C. Then, 5x SDS loading buffer was added into each supernatant, and 12  $\mu$  were subjected to immunoblot analysis. After transfer, the protein was blocked for MAP kinase activation detection with 5% BSA for 1 h. The membrane was then washed three times in TBS-T and incubated overnight at 4 °C in TBS-T and  $\alpha$ -p44/42 MAP kinase (Erk1/2) antibody (1:5,000, CST). After another three washes with TBS-T, the membrane was incubated in  $\alpha$ -rabbit-HRP (1:5,000, Sigma) for 2 h. Phosphorylated MAP kinases 3, 4/11 and 6 were detected using Pierce ECL western blotting substrate (Thermo Fisher).

RIP. Transgenic plants expressing p35S-IRR-3xHA, p35S-IRRS<sup>745A,5747A</sup>-3xHA or p35S-SR45-3xHA constructs were grown in plates containing half-strength MS media for 10–15 days. Transgenic plants expressing the empty vector p35S-3xHA were used as a control. The plants were transferred to half-strength MS liquid media for approximately 16 h before treatment with 1  $\mu$ M AtPep1 for 30 min and 4 h. Approximately 1 g of seedlings were carefully collected and rinsed

with water before crosslinking. The crosslinking was performed by immersing the seedlings in 0.5% formaldehyde and applying a vacuum four times (15 s per time). The seedlings were then kept at room temperature for 10 min, and glycine was added to a final concentration of 83 mM. After this, the seedlings were again subjected to a vacuum four times (15 s per time) and incubated for 5 min to quench the crosslinking. The seedlings were rinsed with water five times, wrapped in a few layers of Kimwipes to remove water and frozen in liquid nitrogen. The nuclear extract preparation was performed as previously described71. To immunoprecipitate the RNA-protein complex, the nuclear extract was resuspended in 900 µl of ChIP dilution buffer (1.1% Triton X-100, 1.2 mM EDTA, 16.7 mM Tris-HCl, pH 8.0, 167 mM NaCl and 160 units per ml of RnaseOUT) and centrifuged at 16,000 g for 10 min at 4 °C. The supernatant was transferred to a clean microcentrifuge tube, and a small aliquot of the supernatant was removed to probe as RNA inputs. Thirty microlitres of anti-HA magnetic beads (Sigma) per sample was prepared by washing the beads five times with 1 ml Binding/ Washing buffer (150 mM NaCl, 20 mM Tris-HCl, pH 8.0, 2 mM EDTA, 1% Triton X-100 and 0.1% SDS). The beads were resuspended in 50 μl of Binding/Washing buffer per sample and added to the diluted nuclear extraction. The samples were incubated on a rotator for 3h at 4°C. The anti-HA magnetic beads were washed six times with 1 ml of Binding/Washing buffer containing 40 units per ml RnaseOUT and the magnetic separation rack. To elute the protein-RNA complexes, 60 µl of RIP Elution buffer (100 mM Tris-HCl, pH 8.0, 10 mM EDTA, 1% SDS and 800 units per ml RnaseOUT) was added to the beads, and the tubes were incubated on a rotator at room temperature for 10 min. The supernatant was saved. The elution was repeated with an additional 60 µl of RIP Elution buffer at 65 °C for 10 min. The supernatants from both elution steps were combined. At the same time, 110 µl of RIP elution buffer was added to the 10 µl of RNA input sample. An aliquot of 1.2 µl Proteinase K (20 mg ml<sup>-1</sup>, Invitrogen) was added to each IP or input sample. The tubes were incubated at 65 °C for 1 h. The RNA was isolated using Trizol reagent (Life Technologies). To facilitate RNA precipitation, 20 µg of glycogen was added to the aqueous phase before the isopropanol precipitation. The RNA samples were further treated using a Turbo DNA-free kit (Ambion) and cleaned with the RNeasy MiniElute Kit (Qiagen). The RNA was eluted into 15 µl of RNase-free water. The cDNA synthesis and PCR reaction were performed as described in the Supplementary Methods.

In vitro kinase assay. Synthetic cDNA encoding either canonically spliced CPK28 or the CPK28-RI splice variant were made by Genscript. The BIK1 coding region was amplified from the cDNA of Arabidopsis. To generate the BIK1  $^{\rm K105A/K106A}$  kinase-dead mutant, the QuickChange II XL site-directed mutagenesis kit (Agilent Technologies) was used. All fragments were amplified by PCR and fused to GST in the N terminus of pGEX6P-1 vector using the USER enzyme (New England Biolabs). BIK1 and BIK1  $^{\rm K105A/K106A}$  fragments were also fused to His in the N terminus of pET vector using the In-Fusion HD Cloning Kit (Takara). The primers used are listed in Supplementary Table 4. The GST–CPK28, GST–BIK1 and His–BIK1 variants were expressed and purified from  $E.\ coli$  strain BL21. The in vitro kinase assay was performed in reaction buffer (50 mM Tris–HCl pH 7.5, 10 mM MgCl2, free  $Ca^{2+}$  (0, 0.5, 2 and 100  $\mu$ M) buffered by 1 mM EGTA and CaCl2, 1 mM dithiothreitol, 0.1% (v/v) Triton X-100, 200  $\mu$ M cold ATP and 1  $\mu$ Ci ( $\gamma$ -32P)-ATP) at room temperature for 30 min.

VIGS in maize. A VIGS system derived from FoMV was used to induce gene silencing in maize line B73. The 251- and 301-bp gene fragments of GRMZM2G132936 (*ZmIRR*) were amplified by the primers listed in Supplementary Table 4 and cloned into *XhoI/XbaI* sites of the FoMV plasmid in an antisense orientation as described previously<sup>41</sup>, yielding the plasmids pFoMV-IRR-1 and pFoMV-IRR-2. Seven-day-old maize plants were inoculated with both plasmids by a biolistic particle delivery system using gold particles (Seashell Technology). The control plants were biolistically inoculated with FoMV vector carrying no insert (FoMV-V). To confirm FoMV infection and gene silencing in the plants, the total RNA was extracted from the fifth leaf of these plants using Trizol reagent (Life Technologies). cDNA was synthesized, and PCR using primers designed to amplify a specific fragment from the FoMV genomic RNA was performed. The relative expression levels of *ZmIRR* were evaluated by qRT-PCR, using *ZmRLP17* as a reference gene. The primers used are listed in Supplementary Table 4.

Volatile emission assay. The fifth maize leaf was excised using a razor blade and supplied with either 1 ml of water or  $5\,\mu M$  ZmPep3 solution through the petiole overnight for 16 h. The leaves were collected and individually kept in closed glass tubes for 1 h under the light while volatiles were collected on 50 mg of Super Q (80/100 mesh; Alltech). Volatile compounds were eluted with methylene chloride containing nonyl acetate as an internal standard, and analysed by gas chromatography as described previously  $^{72}$ .

Further information on the research methods is available in the Supplementary Information.

**Reporting Summary.** Further information on research design is available in the Nature Research Reporting Summary linked to this article.

### Data availability

The raw read sequences are deposited in the National Center for Biotechnology Information Gene Expression Omnibus (http://www.ncbi.nlm.nih.gov/geo/) under the accession number GSE146282. The data generated and analysed in this study are included in the published article and Supplementary Information. All data are available from the corresponding author upon request.

Received: 1 August 2019; Accepted: 11 June 2020; Published online: 20 July 2020

#### References

- Kobayashi, K. S. & Flavell, R. A. Shielding the double-edged sword: negative regulation of the innate immune system. J. Leukoc. Biol. 75, 428–433 (2004).
- Gassmann, W. Alternative splicing in plant defense. Curr. Top. Microbiol. Immunol. 326, 219–233 (2008).
- Liu, J., Qian, C. & Cao, X. Post-translational modification control of innate immunity. *Immunity* 45, 15–30 (2016).
- Xu, G. et al. Global translational reprogramming is a fundamental layer of immune regulation in plants. *Nature* 545, 487–490 (2017).
- Nuhse, T. S., Bottrill, A. R., Jones, A. M. & Peck, S. C. Quantitative phosphoproteomic analysis of plasma membrane proteins reveals regulatory mechanisms of plant innate immune responses. *Plant J.* 51, 931–940 (2007).
- Withers, J. & Dong, X. Post-translational regulation of plant immunity. Curr. Opin. Plant Biol. 38, 124–132 (2017).
- Tena, G., Boudsocq, M. & Sheen, J. Protein kinase signaling networks in plant innate immunity. Curr. Opin. Plant Biol. 14, 519–529 (2011).
- 8. Lu, D. et al. Direct ubiquitination of pattern recognition receptor FLS2 attenuates plant innate immunity. *Science* **332**, 1439–1442 (2011).
- Feng, B. et al. Protein poly(ADP-ribosyl)ation regulates Arabidopsis immune gene expression and defense responses. PLoS Genet. 11, e1004936 (2015).
- Macho, A. P. & Zipfel, C. Plant PRRs and the activation of innate immune signaling. Mol. Cell 54, 263–272 (2014).
- 11. Yu, X., Feng, B., He, P. & Shan, L. From chaos to harmony: responses and signaling upon microbial pattern recognition. *Annu. Rev. Phytopathol.* **55**, 109–137 (2017).
- Huffaker, A., Pearce, G. & Ryan, C. A. An endogenous peptide signal in *Arabidopsis* activates components of the innate immune response. *Proc. Natl Acad. Sci. USA* 103, 10098–10103 (2006).
- Huffaker, A., Dafoe, N. J. & Schmelz, E. A. ZmPep1, an ortholog of *Arabidopsis* elicitor peptide 1, regulates maize innate immunity and enhances disease resistance. *Plant Physiol.* 155, 1325–1338 (2011).
- Huffaker, A. et al. Plant elicitor peptides are conserved signals regulating direct and indirect antiherbivore defense. *Proc. Natl Acad. Sci. USA* 110, 5707–5712 (2013).
- Trivilin, A. P., Hartke, S. & Moraes, M. G. Components of different signalling pathways regulated by a new orthologue of *AtPROPEP1* in tomato following infection by pathogens. *Plant Pathol.* 63, 1110–1118 (2014).
- Lee, M. W., Huffaker, A., Crippen, D., Robbins, R. T. & Goggin, F. L. Plant elicitor peptides promote plant defences against nematodes in soybean. *Mol. Plant Pathol.* 19, 858–869 (2018).
- Ruiz, C., Nadal, A., Montesinos, E. & Pla, M. Novel Rosaceae plant elicitor peptides as sustainable tools to control *Xanthomonas arboricola* pv. pruni in Prunus spp. Mol. Plant Pathol. 19, 418–431 (2018).
- Lori, M. et al. Evolutionary divergence of the plant elicitor peptides (Peps) and their receptors: interfamily incompatibility of perception but compatibility of downstream signalling. J. Exp. Bot. 66, 5315–5325 (2015).
- Hander, T. et al. Damage on plants activates Ca<sup>2+</sup>-dependent metacaspases for release of immunomodulatory peptides. Science 363, eaar7486 (2019).
- Yamaguchi, Y., Pearce, G. & Ryan, C. A. The cell surface leucine-rich repeat receptor for AtPep1, an endogenous peptide elicitor in *Arabidopsis*, is functional in transgenic tobacco cells. *Proc. Natl Acad. Sci. USA* 103, 10104–10109 (2006).
- Yamaguchi, Y., Huffaker, A., Bryan, A. C., Tax, F. E. & Ryan, C. A. PEPR2 is a second receptor for the Pep1 and Pep2 peptides and contributes to defense responses in *Arabidopsis. Plant Cell* 22, 508–522 (2010).
- Krol, E. et al. Perception of the *Arabidopsis* danger signal peptide 1 involves the pattern recognition receptor AtPEPR1 and its close homologue AtPEPR2. *J. Biol. Chem.* 285, 13471–13479 (2010).
- Tintor, N. et al. Layered pattern receptor signaling via ethylene and endogenous elicitor peptides during *Arabidopsis* immunity to bacterial infection. *Proc. Natl Acad. Sci. USA* 110, 6211–6216 (2013).
- 24. Ross, A. et al. The *Arabidopsis PEPR* pathway couples local and systemic plant immunity. *EMBO J.* **33**, 62–75 (2014).
- Postel, S. et al. The multifunctional leucine-rich repeat receptor kinase BAK1 is implicated in *Arabidopsis* development and immunity. *Eur. J. Cell Biol.* 89, 169–174 (2010).
- 26. Liu, Z. et al. BIK1 interacts with PEPRs to mediate ethylene-induced immunity. *Proc. Natl Acad. Sci. USA* 110, 6205–6210 (2013).

- Lu, D. et al. A receptor-like cytoplasmic kinase, BIK1, associates with a flagellin receptor complex to initiate plant innate immunity. *Proc. Natl Acad.* Sci. USA 107, 496–501 (2010).
- Schulze, B. et al. Rapid heteromerization and phosphorylation of ligand-activated plant transmembrane receptors and their associated kinase BAK1. J. Biol. Chem. 285, 9444–9451 (2010).
- Roux, M. et al. The Arabidopsis leucine-rich repeat receptor-like kinases BAK1/SERK3 and BKK1/SERK4 are required for innate immunity to hemibiotrophic and biotrophic pathogens. Plant Cell 23, 2440–2455 (2011).
- Li, L. et al. The FLS2-associated kinase BIK1 directly phosphorylates the NADPH oxidase RbohD to control plant immunity. *Cell Host Microbe* 15, 329–338 (2014).
- Lal, N. K. et al. The receptor-like cytoplasmic kinase BIK1 localizes to the nucleus and regulates defense hormone expression during plant innate immunity. *Cell Host Microbe* 23, 485–497 (2018).
- Monaghan, J. et al. The calcium-dependent protein kinase CPK28 buffers plant immunity and regulates BIK1 turnover. Cell Host Microbe 16, 605–615 (2014).
- Wang, J. et al. A regulatory module controlling homeostasis of a plant immune kinase. Mol. Cell 69, 493–504 (2018).
- Walley, J. W. et al. Integration of omic networks in a developmental atlas of maize. Science 353, 814–818 (2016).
- Golovkin, M. & Reddy, A. S. An SC35-like protein and a novel serine/ arginine-rich protein interact with *Arabidopsis* U1-70K protein. *J. Biol. Chem.* 274, 36428–36438 (1999).
- Carvalho, R. F. et al. The *Arabidopsis* SR45 splicing factor, a negative regulator of sugar signaling, modulates SNF1-related protein kinase 1 stability. *Plant* Cell 28, 1910–1925 (2016).
- Zhang, X. N. et al. Transcriptome analyses reveal SR45 to be a neutral splicing regulator and a suppressor of innate immunity in *Arabidopsis* thaliana. BMC Genomics 18, 772 (2017).
- 38. Kadota, Y. et al. Direct regulation of the NADPH oxidase RBOHD by the PRR-associated kinase BIK1 during plant immunity. *Mol. Cell* **54**, 43–55 (2014)
- Asai, T. et al. MAP kinase signalling cascade in *Arabidopsis* innate immunity. Nature 415, 977–983 (2002).
- Zhang, M., Su, J., Zhang, Y., Xu, J. & Zhang, S. Conveying endogenous and exogenous signals: MAPK cascades in plant growth and defense. Curr. Opin. Plant Biol. 45, 1–10 (2018).
- Mei, Y., Zhang, C., Kernodle, B. M., Hill, J. H. & Whitham, S. A. A Foxtail mosaic virus vector for virus-induced gene silencing in maize. *Plant Physiol.* 171, 760–772 (2016).
- Anko, M. L. Regulation of gene expression programmes by serine-arginine rich splicing factors. Semin. Cell Dev. Biol. 32, 11–21 (2014).
- 43. Jeong, S. SR proteins: binders, regulators, and connectors of RNA. *Mol. Cell* **40**, 1–9 (2017).
- Thines, B. et al. JAZ repressor proteins are targets of the SCF(COI1) complex during jasmonate signalling. Nature 448, 661–665 (2007).
- Chung, H. S. & Howe, G. A. A critical role for the TIFY motif in repression of jasmonate signaling by a stabilized splice variant of the JASMONATE ZIM-domain protein JAZ10 in *Arabidopsis. Plant Cell* 21, 131–145 (2009).
- 46. Jabs, T., Tschöpe, M., Colling, C., Hahlbrock, K. & Scheel, D. Elicitor-stimulated ion fluxes and O<sub>2</sub>— from the oxidative burst are essential components in triggering defense gene activation and phytoalexin synthesis in parsley. *Proc. Natl Acad. Sci. USA* 94, 4800–4805 (1997).
- Acharya, B. R. et al. Overexpression of CRK13, an *Arabidopsis* cysteine-rich receptor-like kinase, results in enhanced resistance to *Pseudomonas syringae*. *Plant J.* 50, 488–499 (2007).
- Waese, J. et al. ePlant: visualizing and exploring multiple levels of data for hypothesis generation in plant biology. Plant Cell 29, 1806–1821 (2017).
- 49. Ali, G. S. et al. Regulation of plant developmental processes by a novel splicing factor. *PLoS ONE* **2**, e471 (2007).
- Liese, A. & Romeis, T. Biochemical regulation of in vivo function of plant calcium-dependent protein kinases (CDPK). *Biochim. Biophys. Acta* 1833, 1582–1589 (2013).
- Klimecka, M. & Muszynska, G. Structure and functions of plant calcium-dependent protein kinases. Acta Biochim. Pol. 54, 219–233 (2007).
- Manley, J. L. & Tacke, R. SR proteins and splicing control. *Genes Dev.* 10, 1569–1579 (1996).
- 53. Xing, D., Wang, Y., Hamilton, M., Ben-Hur, A. & Reddy, A. S. Transcriptome-wide identification of RNA targets of *Arabidopsis* SERINE/ ARGININE-RICH45 uncovers the unexpected roles of this RNA binding protein in RNA processing. *Plant Cell* 27, 3294–3308 (2015).
- Carpenter, S., Ricci, E. P., Mercier, B. C., Moore, M. J. & Fitzgerald, K. A. Post-transcriptional regulation of gene expression in innate immunity. *Nat. Rev. Immunol.* 14, 361–376 (2014).
- Yang, S., Tang, F. & Zhu, H. Alternative splicing in plant immunity. Int. J. Mol. Sci. 15, 10424–10445 (2014).

- Howard, B. E. et al. High-throughput RNA sequencing of Pseudomonas-infected Arabidopsis reveals hidden transcriptome complexity and novel splice variants. PLoS ONE 8, e74183 (2013).
- Ling, Z., Zhou, W., Baldwin, I. T. & Xu, S. Insect herbivory elicits genome-wide alternative splicing responses in *Nicotiana attenuata*. *Plant J.* 84, 228–243 (2015).
- Bazin, J. et al. Role of MPK4 in pathogen-associated molecular pattern-triggered alternative splicing in *Arabidopsis*. PLoS Pathog. 16, e1008401 (2020).
- Xu, S. et al. Transportin-SR is required for proper splicing of resistance genes and plant immunity. PLoS Genet. 7, e1002159 (2011).
- Zhang, Z. et al. Splicing of receptor-like kinase-encoding SNC4 and CERK1 is regulated by two conserved splicing factors that are required for plant immunity. Mol. Plant 7, 1766–1775 (2014).
- Huang, J. et al. An oomycete plant pathogen reprograms host pre-mRNA splicing to subvert immunity. Nat. Commun. 8, 2051 (2017).
- Dinesh-Kumar, S. P. & Baker, B. J. Alternatively spliced N resistance gene transcripts: their possible role in tobacco mosaic virus resistance. *Proc. Natl Acad. Sci. USA* 97, 1908–1913 (2000).
- Zhang, X. C. & Gassmann, W. Alternative splicing and mRNA levels of the disease resistance gene RPS4 are induced during defense responses. *Plant Physiol.* 145, 1577–1587 (2007).
- Liu, J. et al. Alternative splicing of rice WRKY62 and WRKY76 transcription factor genes in pathogen defense. *Plant Physiol.* 171, 1427–1442 (2016).
- Feng, F. et al. A Xanthomonas uridine 5'-monophosphate transferase inhibits plant immune kinases. Nature 485, 114–118 (2012).
- Rao, S. et al. Roles of receptor-like cytoplasmic kinase VII members in pattern-triggered immune signaling. Plant Physiol. 177, 1679–1690 (2018).
- Walley, J. W. et al. Reconstruction of protein networks from an atlas of maize seed proteotypes. *Proc. Natl Acad. Sci. USA* 110, E4808–E4817 (2013).
- Supek, F., Bošnjak, M., Škunca, N. & Šmuc, T. REVIGO summarizes and visualizes long lists of Gene Ontology terms. PLoS ONE 6, e21800 (2011).
- 69. Gietz, R. D. & Woods, R. A. in *Yeast Protocol* (ed. Xiao, W.) 107-120 (Humana, 2006).
- 70. Schwessinger, B. et al. Phosphorylation-dependent differential regulation of plant growth, cell death, and innate immunity by the regulatory receptor-like kinase BAK1. *PLoS Genet.* 7, e1002046 (2011).
- Xu, F. & Copeland, C. Nuclear extraction from Arabidopsis thaliana. Bio. Protoc. 2, e306 (2012).

 Schmelz, E. A., Alborn, H. T. & Tumlinson, J. H. The influence of intact-plant and excised-leaf bioassay designs on volicitin- and jasmonic acid-induced sesquiterpene volatile release in *Zea mays. Planta* 214, 171–179 (2001).

#### Acknowledgements

We thank S. A. Whitham (Iowa State University Plant Sciences Institute) for providing the constructs for the VIGS experiments, and A. Groisman (University of California San Diego Department of Physics) for the use of his Biolistic inoculation apparatus. This work was funded by NSF CAREER Award no. 1943591, a Hellman Foundation Fellowship and UC San Diego Start-up funds to A.H. K.D. was additionally funded by Ciências sem Fronteiras/CNPq fellowship no. 200260/2015-4. E.P. was additionally funded by the Cell and Molecular Genetics (CMG) Training Program at the University of California, San Diego. Z.S. and S.P.B. were funded by NSF award no. 1546899.

#### **Author contributions**

A.H. and K.D. conceived the project. K.D. conducted the experiments. A.H. and K.D. analysed the data and wrote the manuscript. P.R.W. performed the MAP kinase assay, confocal microscopy experiments and phylogenetic analysis. E.P. analysed the leaf volatile emissions and helped edit the figures. Y.T. performed the in-gel kinase activity assays. C.V. assisted with the generation of the transgenic plant lines. Z.S. and S.P.B. performed the phosphoproteomic analysis. J.I.S. contributed critical experimental resources.

#### **Competing interests**

The authors declare no competing interests.

#### Additional information

Supplementary information is available for this paper at https://doi.org/10.1038/s41477-020-0724-1.

Correspondence and requests for materials should be addressed to A.H.

Reprints and permissions information is available at www.nature.com/reprints.

**Publisher's note** Springer Nature remains neutral with regard to jurisdictional claims in published maps and institutional affiliations.

 $\ensuremath{{}^{\odot}}$  The Author(s), under exclusive licence to Springer Nature Limited 2020



Corresponding author(s):	Alisa Huffaker
Last updated by author(s):	03/06/2020

# **Reporting Summary**

Nature Research wishes to improve the reproducibility of the work that we publish. This form provides structure for consistency and transparency in reporting. For further information on Nature Research policies, see Authors & Referees and the Editorial Policy Checklist.

$\overline{}$					
Ç	tっ	ıtı	st	т.	$\sim$
- 1	10		<b>~</b> 1	ш	רו

For	all statistical analys	ses, confirm that the following items are present in the figure legend, table legend, main text, or Methods section.				
n/a	Confirmed					
	$\square$ The exact sample size (n) for each experimental group/condition, given as a discrete number and unit of measurement					
	A statement on whether measurements were taken from distinct samples or whether the same sample was measured repeatedly					
	The statistical test(s) used AND whether they are one- or two-sided  Only common tests should be described solely by name; describe more complex techniques in the Methods section.					
	A description of all covariates tested					
$\boxtimes$	A description of any assumptions or corrections, such as tests of normality and adjustment for multiple comparisons					
	A full description of the statistical parameters including central tendency (e.g. means) or other basic estimates (e.g. regression coefficient AND variation (e.g. standard deviation) or associated estimates of uncertainty (e.g. confidence intervals)					
	For null hypothesis testing, the test statistic (e.g. <i>F</i> , <i>t</i> , <i>r</i> ) with confidence intervals, effect sizes, degrees of freedom and <i>P</i> value noted Give <i>P</i> values as exact values whenever suitable.					
$\boxtimes$	For Bayesian analysis, information on the choice of priors and Markov chain Monte Carlo settings					
$\boxtimes$	For hierarchical and complex designs, identification of the appropriate level for tests and full reporting of outcomes					
$\boxtimes$	Estimates of effect sizes (e.g. Cohen's d, Pearson's r), indicating how they were calculated					
	1	Our web collection on <u>statistics for biologists</u> contains articles on many of the points above.				
So	ftware and o	code				
Poli	cy information abo	ut <u>availability of computer code</u>				
Da	Data collection MetaMorph, Microscope Imaging, Microscopy Analysis Software were used to collect confocal images; Image Lab 5.1 t electrophoresis and Western blot images; GC-FID using Agilent ChemStation to collect volatiles data.					
Da	ata analysis	Image J (1.51g) software was used for confocal image analysis and root growth measurements; Microsoft Excel 2003; GraphPad				

For manuscripts utilizing custom algorithms or software that are central to the research but not yet described in published literature, software must be made available to editors/reviewers. We strongly encourage code deposition in a community repository (e.g. GitHub). See the Nature Research guidelines for submitting code & software for further information.

QuickCalcs and GraphPad Prism 8.0 (GraphPad Software, Inc.) for statistical analyses; MEGA7 for phylogenetic tree analysis; BioRad CFX96 program to determine the threshold cycle for qRT-PCR analysis; REViGO for Gene Ontology terms analysis; GC-FID data was

# Data

Data analysis

Policy information about availability of data

All manuscripts must include a data availability statement. This statement should provide the following information, where applicable:

- Accession codes, unique identifiers, or web links for publicly available datasets
- A list of figures that have associated raw data
- A description of any restrictions on data availability

RNA-Seq data associated with Figure 3 has been deposited in NCBI GEO for release on 05/03/2020. The accession number is GSE146282. Updated information for IRR gene annotation will be submitted to TAIR and MaizeGDB upon publication. All figures have associated raw data available upon request.

analyzed using Agilent MassHunter Workstation Software vB.08.00.

Field-specific reporting				
Please select the or	ne below tha	at is the best fit for your research. If you are not sure, read the appropriate sections before making your selection.		
Life sciences		Behavioural & social sciences		
For a reference copy of t	the document w	vith all sections, see <a href="mailto:nature.com/documents/nr-reporting-summary-flat.pdf">nature.com/documents/nr-reporting-summary-flat.pdf</a>		
Life scier	nces s	tudy design		
All studies must dis	sclose on the	ese points even when the disclosure is negative.		
Sample size	A minimum sample size of 3 independent biological replicates was selected.			
Data exclusions	No data exclusions were made.			
Replication	Experiments were perfomed at least two times with similar results.			
Randomization	Pots with plants were randomized in the growth room, and sample orders were randomized during analysis.			
Blinding	For some experiments, samples and treatments were analyzed blindly and comparisons were made only in the end.			
Reporting for specific materials, systems and methods  We require information from authors about some types of materials, experimental systems and methods used in many studies. Here, indicate whether each material,				
system or method list	ted is relevant	t to your study. If you are not sure if a list item applies to your research, read the appropriate section before selecting a response.		
Materials & exp	perimenta	al systems Methods		
n/a Involved in the study		n/a Involved in the study		
Eukaryotic cell lines Flow cytometry				
Palaeontology MRI-based neuroimaging				
Animals and other organisms				
Human research participants				
Clinical data				
Antibodies				
Antibodies used		Anti-phosphoserine (Sigma), anti-mouse-HRP-conjugated secondary antibody (Sigma), anti-p44/42 MAPK (Erk1/2) antibody (CST), anti-rabbit-HRP (Sigma), anti-HA (Sigma)		

Validation

- 1) Anti-phosphoserine (Sigma, AB1603) https://www.sigmaaldrich.com/catalog/product/mm/ab1603?lang=en&region=US
- 2) Anti-p44/42 MAPK (Erk1/2) antibody (#9101, CST), https://www.cellsignal.com/products/primary-antibodies/phosphop44-42-mapk-erk1-2-thr202-tyr204-antibody/9101
- 3) Monoclonal Anti-HA antibody produced in mouse, clone HA-7, purified from hybridoma cell culture (Sigma # H3663-200UL) https://www.sigmaaldrich.com/catalog/product/sigma/h3663?lang=en&region=US